Articles in PresS. J Neurophysiol (March 14, 2012). doi:10.1152/jn.00977.2011

Title:

The relationship between voltage-sensitive dye imaging signals and spiking activity of neural populations in primate V1

Authors:

Yuzhi Chen[1], Chris R. Palmer[1], and Eyal Seidemann

Dept. of Psychology and Center for Perceptual Systems, University of Texas at Austin

Austin, TX 78712, USA

[1] These authors contributed equally to this work

Running Head:

Relationship between VSDI signals and spiking activity

Corresponding author:

Eyal Seidemann

The University of Texas at Austin

Dept. of Psychology and Center for Perceptual Systems,

108 East Dean Keeton

1 University Station A8000

Austin, TX 78712-0187

Phone (512) 232-6052

Fax (512) 471-7356

eyal@mail.cps.utexas.edu

Copyright © 2012 by the American Physiological Society.

Abstract

Voltage sensitive dye imaging (VSDI) is a powerful technique for measuring neural population responses from a large cortical region simultaneously with millisecond temporal resolution and columnar spatial resolution. However, the relationship between the average VSDI signal and the average spiking activity of neural populations is largely unknown. To better understand this relationship, we compared visual responses measured from V1 of behaving monkeys using VSDI and single-unit electrophysiology. We report large and systematic differences between position and orientation tuning properties obtained with these two techniques. We then show that a simple computational model can explain these tuning differences. This model, together with our experimental results, allowed us to estimate the quantitative relationship between the average VSDI signal and local spiking activity. We find that this relationship is similar to the previously reported nonlinear relationship between average membrane potential and spike rate in single V1 neurons, suggesting that VSDI signals are dominated by sub-threshold synaptic activity. This model, together with the VSDI measured maps for spatial position (retinotopy) and orientation, also allowed us to estimate the spatial integration area over which neural responses contribute to the VSDI signal at a given location. We find that the VSDI-integration area is consistent with a Gaussian envelope with a space constant of ~230 μm. Finally, we show how this model and estimated parameters can be used to predict the pattern of population responses at the level of spiking activity from VSDI responses.

Key words: voltage-sensitive dye imaging, nonlinear transfer function, spatial integration, topographic maps, mammalian cortex

Introduction

A fundamental feature of early sensory cortical areas is the representation of sensory information in two-dimensional (2-D) topographic maps across the cortical surface (e.g., (Woolsey 1952; Mountcastle 1957; Hubel and Wiesel 1963)). Within these maps, sensory stimuli elicit patterns of neural responses that are distributed across multiple square millimeters. Characterizing these patterns in space and in time is therefore a prerequisite to understanding sensory encoding and decoding.

Voltage-sensitive dye imaging (VSDI) provides a powerful tool for measuring 2-D patterns of population responses in the superficial cortical layers at high spatial and temporal resolution *in vivo* (reviewed in (Grinvald and Hildesheim 2004)). Furthermore, VSDI can be applied to behaving animals performing demanding perceptual tasks, where sensory encoding and decoding can be studied most directly (e.g., (Chen, Geisler et al. 2006)). However, the interpretation of VSDI findings is complicated by open questions regarding the quantitative relationship between the average VSDI-measured neural signals and the average patterns of population responses at the level of spiking activity.

Specifically, two key questions regarding the relationship between VSDI signals and spiking activity *in vivo* remain open. First, what is the relative contribution of subthreshold and suprathreshold neural responses to VSDI signals? While in single neurons, VSDI signals are directly proportional to membrane voltage across the entire physiological dynamic range (e.g., (Salzberg, Davila et al. 1973)), at the level of neural populations, factors such as spiking activity in non-myelinated axons and back-propagation of action potentials from cell body into the dendrites could lead to a significant contribution of spikes to the VSDI signal. A central goal of the current study is to estimate the relative contribution of these factors to VSDI signals *in vivo*.

70 Second, what is the size of the neural population that contributes to the VSDI signal at a given cortical
71 location? This VSDI integration area depends on the horizontal spread of dendrites and axons in the
72 cortex, on the light scattering properties of the cortical tissue and on the optical properties of the
73 imaging system, but the relative contribution of these factors and the final value of this integration area
74 are unknown. A second goal of the current study was to provide an estimate of the VSDI integration
75 area.

76 To begin to address these open questions, we measured neural responses from V1 of behaving monkeys
77 using a combination of VSDI and extracellular electrophysiology. Specifically, we compared the average
78 tuning properties of VSDI signals and single-unit (SU) spiking activity across two stimulus dimensions –
79 orientation and spatial position.

80 Because subthreshold membrane potentials are generally less selective and more broadly tuned than
81 spiking activity (reviewed in (Priebe and Ferster 2008)), the relative contribution of subthreshold vs.
82 suprathreshold responses to the VSDI signal must affect the relationship between the tuning properties
83 of signals measured with these two techniques. A larger contribution of subthreshold responses to the
84 VSDI signals will necessarily lead to broader tuning and decreased selectivity of the VSDI-measured
85 responses relative to the spiking activity of single V1 neurons. By taking into account the known
86 relationship between average membrane potential and average spiking activity in single V1 neurons, our
87 first goal was to obtain an estimate of the relative contribution of sub- and supra-threshold responses to
88 the VSDI signal.

89 In addition, the tuning properties of the VSDI-measured neural responses depend on the size of the
90 neural population that contributes to the VSDI signal at a given location. V1 contains topographic maps
91 of spatial position (i.e., retinotopy (Talbot and Marshall 1941; Daniel and Whitteridge 1961; Tootell,
92 Silverman et al. 1982; Van Essen, Newsome et al. 1984; Tootell, Switkes et al. 1988; Adams and Horton

2003) and orientation (Hubel and Wiesel 1963; Hubel and Wiesel 1968; Blasdel and Salama 1986; Bonhoeffer and Grinvald 1991; Obermayer and Blasdel 1993)). Consider, for example, tuning for orientation. Intuitively, an increase in the VSDI integration area will lead neurons with different preferred orientations to contribute to the VSDI signal at a given location. This, in turn, would lead to broadening of the orientation tuning of the VSDI-measured responses relative to the average tuning of individual V1 neurons. In addition, an increase in the VSDI integration area will lead to an increase in the component of the response that is not orientation selective (untuned component). VSDI allows us to measure both the retinotopic map (Fig. 2; (Yang, Heeger et al. 2007)) and the orientation map (Fig. 6) with high precision and reliability in the awake monkey. Therefore, we can use these maps to estimate how different VSDI integration areas are expected to affect the average tuning properties of the VSDI-measured responses for orientation and position. By comparing these predictions with the observed VSDI tuning curves, our second goal was to obtain an estimate of the VSDI integration area.

To address these goals, we developed a simple computational model that attempts to predict the pattern of population responses at the level of spiking activity from the VSDI signals, and vice versa. The model includes two free parameters; one for the relative contribution of sub- and supra-threshold responses to the VSDI signals and one for the VSDI integration area. We then used our measured tuning curves, together with the VSDI-measured topographic maps for spatial position and orientation, to constrain our model. The results of this analysis show that VSDI signals are dominated by subthreshold synaptic activity, and that the space constant of the Gaussian-shaped VSDI integration area is ~230 µm. Because a single set of parameters accounts for our results across the two stimulus dimensions, our study raises the possibility that for a wide range of visual stimuli, the average pattern of population responses at the level of spiking activity could be predicted from the VSDI signals.

116 # Methods

117 **Subjects and surgery**

118 Results from a total of eight monkeys (Macaca mulatta) were included in this study: six contributed to
119 position tuning measurements (3 for electrophysiology and 3 for VSDI); six contributed to orientation
120 tuning measurements (3 for electrophysiology, 1 for VSDI and 2 for both); four contributed to both
121 position and orientation tuning measurements. Surgical procedures for VSDI and electrophysiological
122 recordings from behaving monkeys have been described in detail elsewhere (Chen, Geisler et al. 2006;
123 Palmer, Cheng et al. 2007; Chen, Geisler et al. 2008). All surgical procedures were performed under
124 deep anesthesia, using strictly sterile techniques, in a dedicated surgical suite. All procedures were
125 approved by the University of Texas Institutional Animal Care and Use Committee and conformed to
126 National Institutes of Health standards.

127 **Task**

128 Each trial began when the animal achieved fixation in a small window (<2° full width) around a 0.1 X 0.1°
129 central fixation point displayed against a uniform gray background. Following initial fixation, a visual
130 stimulus (either Gabor patch or sinusoidal grating, see details below) was presented parafoveally to both
131 eyes for 1-2 seconds. The monkey received a reward at the end of the stimulus presentation interval
132 provided it did not break fixation.

133 **Visual stimulus for position tuning**

134 For position tuning (electrophysiology and VSDI), the visual stimulus was a small Gabor patch (a
135 sinusoidal grating in a Gaussian envelope). The Gabor patch was presented 2 to 4 times at 2 Hz (200 ms
136 on and 300 ms off). The position of the Gabor patch varied pseudo-randomly from trial to trial among a
137 total of 5 to 8 positions (extending from receptive field (RF) center, or a location within the imaging

138 chamber close to the representation of the fovea in the case of the VSDI experiments, to a peripheral
139 location that elicited a response indistinguishable from the baseline). In different experiments stimulus
140 position was changed along horizontal, vertical, or iso-eccentric directions (for electrophysiology only).
141 The contrast of the Gabor patch was 100% and it was in sine phase. In electrophysiological recordings
142 the spatial frequency and orientation of the Gabor patch were adjusted to match the preferred
143 parameters of the recorded neuron (mean RF eccentricity, 2.57°; range across experiments, 2.01 – 3.17°;
144 mean spatial frequency, 2.73 cycles per degree (cpd); range, 2 – 4.2 cpd; no orientation bias), while the
145 space constant (σ) of the Gabor patch was kept constant at 0.167°. In VSDI experiments, only the
146 position of the Gabor patch varied across experiments (mean eccentricity, 2.55°; range across
147 experiments, 1.8 – 3.35°); the parameters of the Gabor patch were kept constant (σ=0.167°; spatial
148 frequency=2.76 cpd; orientation=0°).

149 **Visual stimulus for orientation tuning**

150 For orientation tuning, the visual stimulus was either a small Gabor patch (electrophysiology) flashed 2
151 to 4 times at 2 Hz (200 ms on and 300 ms off), or a larger sinusoidal grating (VSDI) flashed at 5 Hz (60 ms
152 on and 140 ms off) for 1 second. The 5 Hz stimulus presentation helped us obtain an improved signal-to-
153 noise ratio necessary for VSDI measurements of high-resolution orientation maps (see Fig. 5 and Results
154 section on orientation tuning of VSDI signals). The orientation the stimulus varied from 0° to 180° in
155 steps of 15° or 30°. In electrophysiological recordings, the position, spatial frequency and size of the
156 Gabor patch were adjusted to match the preferred parameters of the recorded neuron. The grating
157 stimulus used in the VSDI experiments always fully covered the visual field corresponding to the V1 area
158 in the imaging chamber, and the spatial frequency and size of the grating were kept constant at 2 cpd
159 and 6°, respectively.

160 Visual stimuli were presented on a gamma-corrected high-end 21 inch color display at a fixed mean
161 luminance of 30 cd/m^2. The display subtended 20.5 X 15.4° at a viewing distance of 108 cm, had a pixel
162 resolution of 1024 X 768, 30-bit color depth, and a refresh rate of 100 Hz.

163 **Electrophysiology**

164 Our electrophysiological recording techniques have been described previously (Palmer, Cheng et al.
165 2007). Briefly, electrodes (FHC, Bowdoinham, ME) were advanced using a guide tube through a rubber
166 gasket that sealed a small hole in the transparent plastic cover sealing the recording chamber. A dual
167 slope/height window discriminator (Bak Electronics, Germantown, MD) was used to isolate spikes from
168 single neurons. Only waveforms that were well separated from the background noise were considered
169 single units.

170 After isolation, we used a custom software package (courtesy of G. DeAngelis, University of Rochester,
171 Rochester, NY) to qualitatively analyze the receptive field properties of the recorded neuron. The
172 software allowed interactive variation of the parameters (location, spatial frequency, orientation, and
173 size) of a sinusoidal grating while graphically monitoring neural responses. Based on the initial analysis
174 of the receptive field properties, we performed an additional quantitative assessment using a Gabor
175 presented for 200 ms for a minimum of five trials per condition to identify the preferred orientation of
176 the neuron. We also quantitatively assessed the preferred size (at a fixed spatial frequency of 3 cpd) and
177 spatial frequency (with size fixed at the preferred value) of some of the recorded neurons.

178 **Voltage sensitive dye imaging**

179 The experimental techniques for VSDI in awake, behaving monkeys have been described elsewhere
180 (Arieli and Grinvald 2002; Arieli, Grinvald et al. 2002; Seidemann, Arieli et al. 2002; Slovin, Arieli et al.
181 2002). Briefly, in the current study we used the voltage sensitive dyes RH1838 or RH1691 (Shoham,

182 Glaser et al. 1999), and a high speed camera (Imager 3001, Optical Imaging), to image any changes in
183 membrane potentials in an area of up to 16 x 16 mm^2 over the occipital lobe of macaque monkeys.
184 Results from the two dyes were combined because no systematic differences between signals obtained
185 with these two dyes were observed. The camera collected 512 x 512 pixels at 110 Hz. For position tuning
186 measurements, imaging area was 16 x 16 mm^2 with pixel size of ~32 x 32 μm^2. For orientation tuning
187 measurements, imaging area was 5 x 5 mm^2 with pixel size of ~10 x 10 μm^2.

188 **Behavior monitoring and data acquisition**

189 Behavior monitoring and data acquisition were performed by a computer running software for real-time
190 neurophysiological recordings from alert animals (Tempo; Reflective Computing, St. Louis, MO). This
191 computer interfaced with an infrared eye-tracker (Dr. Bouis Devices, Karlsruhe, Germany) for high-
192 quality analog eye position monitoring. Eye position signals were sampled with 16-bit resolution at 1
193 kHz. Electrophysiological signals were sampled at 1 kHz. The data acquisition computer also interfaced
194 with the systems used to acquire electrophysiological data (Bak Electronics, Mount Airy, MD) and optical
195 imaging data (Optical Imaging, New York). In addition, this computer controlled a dedicated PC with a
196 high-end graphics card that was used for stimulus presentation.

197 **Experiment database for position tuning**

198 The results are based on 19 SU recordings and 68 VSDI recording sites from 13 VSDI experiments (two of
199 which were performed simultaneously with electrophysiology). All electrophysiological recordings had
200 to meet three criteria to be included in our analysis: (1) minimum of eight repetitions per condition; (2)
201 peak stimulus-evoked response >5 spikes/sec; (3) eccentricity of RF center between 1.8 and 3.4°. Of the
202 37 single neurons that were initially screened, 6 were excluded because isolation was not maintained for
203 long enough to collect the minimum number of repeats, 1 was excluded due to the weak peak stimulus-

evoked response, and 11 were excluded because their RF centers were outside the required eccentricity range.

For VSDI recordings, we usually had 8 sites (corresponding to 8 stimulus positions) in each experiment. Three criteria were applied to these sites: (1) peak d' >3 (see below); (2) spatial response had to be fully within the imaged V1 area and sufficiently far from V2; (3) stimulus eccentricity between 1.8 and 3.4°. Of the total 102 sites tested, 15 were excluded due to a low peak d', 4 due to proximity to V2, and 15 because they were outside the required eccentricity range.

Experiment database for orientation tuning

The results are based on 44 SU recordings and 8 VSDI experiments. All electrophysiological recordings had to meet two criteria to be included in our analysis: (1) minimum of eight repetitions per condition; (2) peak stimulus-evoked response >5 spikes/sec. Of the 73 single neurons we initially recorded, 17 were excluded because the number of repetitions per condition was too low, and 12 were excluded due to the weak stimulus-evoked response.

For VSDI recordings, the criterion was that d' was greater than 8 for > 90% of the 8 x 8 binned pixels within a rectangular area larger than one quarter of entire imaged area.

Analysis of electrophysiological data

For both position tuning and orientation tuning, SU responses (spikes) were averaged during a 200 ms interval starting 36 ms after stimulus onset. The results were essentially identical when averaging the responses in 100 ms intervals starting at 36 ms or at 136 ms after stimulus onset (data not shown). Responses for a given trial were then averaged across the 2-4 stimulus presentations.

Analysis of the voltage sensitive dye imaging

For position tuning, VSDI analysis followed eight steps: (i) remove outlier trials (see below) from each block, usually less than 1% of trials; (ii) normalize to fractional change relative to the average fluorescence at each location across all trials; (iii) average signals across all trials for each stimulus condition; (iv) subtract the mean blank condition; (v) subtract from the responses in each condition the average response in the 100 ms interval prior to response onset; (vi) average the VSDI response during the integration period (36 to 236 ms after stimulus onset); (vii) fit the averaged VSDI response with a 2-D Gaussian function with DC and (viii) remove the fitted DC component. The VSDI spatial position tuning curves were slightly narrower when averaging the responses in a 100 ms interval starting at 36 ms than when averaging the responses in a 100 ms interval starting at 136 ms after stimulus onset, but this difference had negligible effect on our results (data not shown). Effective pixel size for position tuning experiments (after 8 X 8 binning) was ~250 µm. Steps ii-vi were done independently for each 8 X 8 binned pixel. VSDI responses were averaged across the 2 stimulus presentations per trial. To remove outliers (step i), we first divided each frame to four quadrants and averaged the grey level in each quadrant. Outliers were trials whose average grey level at any quadrant during any frame exceeded 5 SD from the mean across all trials. Generally, outliers were caused by excessive movements of the animal. Normalization (step ii) and anchoring (step v) were helpful for eliminating the effect of uneven illumination in the recording chamber or uneven dye penetration, and for eliminating the effect of slow drift in the VSDI response across trials. All data analysis was performed in Matlab (Mathworks).

For orientation tuning, VSDI analysis followed eight steps. The first four steps were identical to the ones in the analysis of position tuning (see above). The additional steps were: (v) extract the Fourier transform (FT) amplitude at 5 Hz at each pixel for each condition; (vi) perform 2-D spatial FT on the 5 Hz amplitude map for each condition and extract the components at spatial frequencies between 0.8 and 3 cycle/mm by removing all other frequencies and applying the inverse FT to the filtered data. These components correspond to the VSDI signals shown in Figure 6C; (vii) use a vector-summation method to

calculate the orientation map in Figure 6D; (viii) calculate the orientation tuning curve (Fig. 6F) by averaging orientation tuning across space and adding the average DC components of the 2-D spatial FT. Step v significantly enhances the VSDI signal-to-noise ratio as shown in Fig. 5; step vi can help to reduce the corruption of the orientation map by low spatial frequency noise and high frequency shot-noise (see Fig. 5).

Correcting for the effect of stimulus size on the estimated position tuning widths

Our position tuning width measurements depend on the RF size of the recorded neurons as well as on the stimulus size. To correct for the effect of stimulus size, we used the following equation:

$\sigma_{RF} = \sqrt{\sigma_{Pos}{}^2 - \sigma_{Stim}{}^2}$, where σ_{Stim} is the Gabor stimulus' space constant (0.167°) (for additional details, see (Palmer, Chen et al. 2012)).

Estimating the parameters of the transfer function and integration function

A detailed description of the model is given in Results. Briefly, the model includes a transfer function that describes the non-linear relationship between average spiking activity and average VSDI signal in a small cortical region, and an integration (or blurring) function that describes the region over which neural responses contribute to the VSDI signals at a given location. The transfer function was assumed to be a power function with an exponent N, and the integration function a Gaussian with a space constant σ_{Int} .

For position tuning, both SU and VSDI signals were assumed to follow a Gaussian function over space. Therefore, there is a constant relationship between the power *N* of the transfer function that relates VSDI signals and spiking activity (see Results) and the σs of the Gaussians: $\sigma_{VSDI} = \sqrt{N} \times \sigma_{SU}$. To estimate *N* and its variability, we bootstrapped σ_{VSDI} and σ_{SU} from our measured data sets. As will be

shown later, because the spatial scale of σ_{Int} is much smaller than the spatial scale of the population receptive field, σ_{Int} could not be reliably estimated from the measured position tuning data (see Results).

For orientation tuning, we adopted a curve fitting method to estimate the two parameters. We first obtained the average orientation tuning curve of SU by bootstrapping the SU data set. Then, we randomly picked an orientation map from the 8 VSDI experiments, and assigned the average orientation tuning curve of SU to each pixel in the map. Specifically, we aligned the peak of the curve to the preferred orientation at each pixel, and then used the tuning amplitude at that pixel to scale the tuning amplitude of the curve. This allowed us to mimic the orientation response of SU over the cortex while ensuring that the average orientation tuning was the same as the one obtained from the SU recordings. Next, we applied the transfer function to convert these cortical orientation responses of SUs to membrane potentials, and integrated the membrane potentials with a Gaussian function to obtain the predicted VSDI signals at each pixel. Finally, the orientation tuning curve was calculated from the simulated VSDI signals using the method applied to the real VSDI recordings. The curve fitting method adjusted the power *N* of the transfer function and the space constant σ_{Int} of the integration function to minimize the least square error between the model's prediction and the measured average VSDI tuning curve.

In addition, to verify that our estimated model parameters do not depend on the assumption that all V1 neurons have identical tuning curve widths, we repeated the analysis described above but allowed the orientation tuning width at each location to be a random sample from a Gaussian distribution with mean of 23° and SD of 10°. The estimated parameters in this analysis were indistinguishable from those in the previous analysis.

293 # Results

294 We begin our results section by describing the average spatial and orientation tuning properties of V1
295 responses measured with VSDI and single-unit spiking activity. We then develop a simple computational
296 model that predicts the expected VSDI tuning curves for position and orientation from the average
297 tuning curves of individual V1 neurons and from the retinotopic and orientation maps. By comparing the
298 model's predictions with the observed VSDI tuning curves, we obtain estimates of the relative
299 contribution of sub- and supra-threshold responses to the VSDI signals and of the VSDI integration area.

300

301 **Position tuning of single V1 neurons**

302 To measure the position tuning of V1 neurons, we systematically varied the position of a small Gabor
303 patch (σ=0.167°; optimal orientation and spatial frequency; contrast = 100%) relative to the center of
304 the neuron's receptive field (RF). Stimulus position was varied along a linear trajectory (horizontal, n=2;
305 vertical, n=14) or an iso-eccentric trajectory (n=3), starting at the center of the neuron's RF (n=16) or
306 extending in both directions from RF center (n=3). Figure 1B shows the responses of one V1 neuron to 7
307 stimulus positions that varied along a vertical trajectory (Fig. 1A). The response dropped rapidly as
308 stimulus position shifted away from RF center. We plotted the average firing rate as a function of the
309 distance between stimulus center and RF center to obtain the position tuning curve (Fig. 1C). To
310 estimate position tuning width, we fitted the position tuning data with a half-Gaussian. The space
311 constant (σ) of the Gaussian in this case was 0.30°. The position tuning curve is closely related to the
312 neuron's RF profile. Because RF size of V1 neurons depends on eccentricity (e.g., (Hubel and Wiesel
313 1974; Van Essen, Newsome et al. 1984)), we restricted our analysis to a narrow range of eccentricities
314 (1.8°-3.4°).

315 Figure 3A (left bar) shows the average position tuning space constants across all recorded neurons after
316 correcting for the effect of stimulus size (see Methods). The average position tuning width of our single
317 V1 neurons is 0.25°±0.03 (± values indicate standard error of the mean (SEM) throughout this paper),
318 comparable to previous measurements at similar eccentricities (e.g., (Levitt and Lund 2002 ; Read and
319 Cumming 2003; Nienborg and Cumming 2006)).

320

321 **Position tuning of VSDI signals in V1**

322 To obtain analogous position tuning curves for VSDI signals, we measured the VSDI response maps to
323 Gabor stimuli that varied in position along a linear trajectory (horizontal, n=34; vertical, n=34). Figure 2
324 shows the response to Gabor stimuli at 6 positions (Fig. 2A) imaged over an area of about 16x16 mm^2
325 (Fig. 2B) in one VSDI experiment. Each Gabor stimulus elicited an ellipsoidal cortical response that was
326 well fitted by a 2-D Gaussian (Fig. 2C), consistent with our previous findings (Chen, Geisler et al. 2006;
327 Chen, Geisler et al. 2008; Palmer, Chen et al. 2012). The position of the active region shifted along the
328 cortical surface as predicted by the retinotopic map in V1 (Fig. 2B). To obtain a position tuning curve, we
329 picked a cortical location corresponding to the center of one stimulus, and measured the responses at
330 this fixed cortical location to stimuli at all possible positions along the trajectory. By plotting the VSDI
331 response as a function of the distance of each stimulus from the center location, we obtained a position
332 tuning curve analogous to the position tuning curves of single V1 neurons. We repeated this analysis for
333 each stimulus position that fell within our limited eccentricity range. Figure 2D shows the position
334 tuning curves obtained at all 6 stimulus locations. Similar to the SU data, the position tuning curves were
335 fitted with a Gaussian. The space constants estimated with VSDI tended to be larger than the space
336 constants of single V1 units at similar eccentricities.

Figure 3A (right bar) shows the average position tuning space constants for all VSDI sites after correcting for the effect of stimulus size (see Methods). The average VSDI position tuning width is 0.49±0.02°, significantly larger than the tuning width of single V1 neurons ($p<0.001$; t-test). Therefore, average position tuning space constants obtained with VSDI are about twice those obtained with SU electrophysiology (Fig. 3B).

Possible effect of fixational eye movements on position tuning

Because of the proximity of the recorded V1 area to the fovea, small fixational eye movements could lead to significant biases in our estimates of the position tuning data. To test for such an effect in our SU measurements, we computed two eye movement metrics: 1) to capture eye movements within trials, we computed the standard deviation (SD) of the eye position during the stimulus presentation interval and averaged this value across trials; 2) to capture the scatter in the average eye position across trials, we measured the distance of the mean eye position during the stimulus presentation interval from the fixation point in each trial, and then computed the SD of this offset across trials. The average values of the 'within trial' metric (0.13 ± 0.04°, n = 19) and the 'across trials' metric (0.27 ± 0.08°, n = 19) were small. Furthermore, some of this variability is likely to be due to noise in our eye position measurements rather than due to poor fixation. Nevertheless, to determine if the small amount of variability in eye position had an impact on our results, we compared the average position tuning width in neurons in which the 'within trial' or 'across trials' metrics were above and below their median value across all neurons. The position tuning widths were not significantly different in these two groups for the 'within trial' metric (one tailed t-test, $p = 0.13$; Fig. 3C) and for the 'across trials' metric (one tailed t-test, $p = 0.77$; Fig. 3D), demonstrating that our monkeys maintained tight fixation and that fixational eye movements had a negligible impact on our results.

360 We used the same approach to examine possible effects of fixational eye movements on position tuning
361 in our VSDI measurements. These results, which are presented in a separate study (Palmer, Chen et al.
362 2012), show no significant effects of eye movement on our VSDI position tuning estimates.

363

364 **Orientation tuning of single V1 neurons**

365 To estimate the orientation tuning curves of single V1 neurons, we measured SU responses to small
366 Gabor patches (optimal size and spatial frequency; contrast = 100%) at 6 or 12 evenly spaced
367 orientations. Figure 4A shows the response of an example V1 neuron. The neuron responded most
368 strongly to a 60° oriented Gabor, and the response decreased as stimulus orientation differed from the
369 preferred orientation. The orientation tuning curve (Fig. 4B) was fitted with a circular Gaussian to obtain
370 an orientation tuning width (the SD of the circular Gaussian) of 21.2° and a normalized tuning amplitude
371 (NTA=$(R_{pref}-R_{orthogonal})/R_{pref}$)) of 0.79.

372 The distributions of the orientation tuning widths and normalized tuning amplitudes across the 44
373 recorded V1 neurons are shown in Figure 7A and 7B (one neuron with a flat orientation tuning curve for
374 which the estimated tuning width was ~90° was excluded from the histogram of orientation tuning
375 widths). The average orientation tuning width of single V1 neurons is 23.0±1.6° (Fig. 7C, left column),
376 consistent with previous studies (Devalois, Yund et al. 1982; Vogels and Orban 1990; Nauhaus, Benucci
377 et al. 2008). The average normalized tuning amplitude is 0.77±0.03 (Fig. 7D, left column).

378

379 **Orientation tuning of VSDI signals in V1**

380 Our next goal was to estimate the average orientation tuning curve of VSDI signals. To measure reliable
381 VSDI signals from orientation columns in behaving monkeys, we made two changes to the experimental

protocol we used for measuring position tuning with VSDI. First, to measure signals at the sub-millimeter scale of orientations columns, we zoomed in to a cortical area of 5x5 mm^2 (Fig. 6A), using a magnification that is about 3 times higher than for position tuning measurements (where our goal was to have a large field of view; Fig. 2B). Second, in order to measure the weaker orientation specific VSDI signals, we changed our visual stimulation protocol from 2 Hz stimulus presentation (200 ms on, 300 ms off) to 5 Hz stimulus presentation (60 ms on, 140 ms off).

Increasing the temporal frequency of the visual stimulation from 2 Hz to 5 Hz provided a dramatic increase in the signal-to-noise ratio (S/N) of the VSDI signals. Figure 5 shows a comparison of VSDI responses to stimuli flashed at 2 Hz and 5 Hz. The VSDI signals display clear response modulations at stimulus frequency (Fig. 5A, top panel) as expected for flashed stimuli, with a clear peak at 2 Hz (Fig. 5A, middle panel) and at 5 Hz (Fig. 5B, middle panel). The amplitude of the response tended to be lower in the 5 Hz presentation. However, because the noise in the VSDI signal decreases with frequency (see dashed line in Fig. 5A and B, middle panels; see also (Benucci, Frazor et al. 2007)), the d', or S/N, for 5 Hz presentation was about three times higher than for 2 Hz presentation (Fig. 5A and B, bottom panels; Fig. 5C). In the following analysis of VSDI orientation tuning, we computed the 5Hz Fourier amplitude at each pixel to obtain the spatial responses map for each orientation condition. As shown below, the higher magnification and improved S/N allowed us, for the first time, to measure reliable orientation selective signals with VSDI in behaving monkeys.

To estimate the average orientation tuning curve of VSDI signals, we calculated the spatial response maps to sine-wave gratings at 12 evenly spaced orientations (spatial frequency=2 cycle/°; contrast = 100%). To determine the spatial scale of the orientation selective signals, we first computed the 1-D amplitude spectrum of the response maps to single orientations by radially averaging the 2-D amplitude spectrum of each orientation map, and then averaging the 1-D amplitude spectra across the 12

orientation (Fig. 6B). Orientation selective signals produced a clear peak at ~1.2 cycle/mm (corresponding to a peak period of ~0.83 mm), consistent with previous studies of orientation maps in macaque V1 (Hubel and Wiesel 1968; Blasdel and Salama 1986; Obermayer and Blasdel 1993). To focus on the spatial scale of the orientation columns, we selected a range of spatial frequencies based on the average 1-D amplitude spectrum (dashed vertical lines in Fig. 6B) of 0.8-3 cycle/mm, corresponding to elements with a period of 0.33-1.25 mm. Figure 6C shows the pattern of V1 responses elicited by gratings at 4 of the 12 orientations after spatial filtration. The maps display small sub-millimeter patches, with bright patches responding above average to the given orientation and dark patches responding below average. To determine whether these patches reflect orientation columns, we computed the correlation between pairs of maps as a function of their stimulus orientation difference (Fig. 6E). If these maps reflected filtered noise rather than orientation columns, the correlations between pairs of maps should be close to zero and be independent of the orientation difference. Instead, the correlations between two maps drop systematically as the orientation difference increases, reaching a near zero value when the two orientations differ by 45°, and a maximally negative value of -0.76 for orientation difference of 90°. These results demonstrate that the obtained response maps capture the systematic representation of orientation across the cortical surface in V1. The function relating orientation difference to map correlations (Fig. 6E) becomes flatter when including lower spatial frequencies (0.2-3 cycle/mm, red) or higher spatial frequencies (0.8-5 cycle/mm, blue) in the response maps, indicating that most orientation selective signals in macaque V1 are represented at the scale of 0.8-3 cycle/mm.

Next we used a vector summation method (Tso, Frostig et al. 1990) to obtain a complete orientation map from these single-orientation response maps (Fig. 6D). In this map, color indicates the preferred orientation at each location, while saturation indicates the strength of orientation tuning. A small inset shows the typical pinwheel organization of orientation columns (Bonhoeffer and Grinvald 1991). To the

429 best of our knowledge, these are the first high quality orientation maps obtained with VSDI in behaving
430 monkeys.

431 To estimate the average orientation tuning of the VSDI signal from these orientation maps, we
432 computed the orientation tuning curve at each cortical location, aligned all curves to peak at zero, and
433 then averaged these curves across all locations. Figure 6F shows the average orientation tuning curve
434 for the VSDI signal in this example experiment. The orientation tuning width (σ=35.7°) is broader than
435 the average value for single V1 units, and the normalized tuning amplitude (NTA=0.09) is much smaller
436 than the average NTA value for single V1 units. The average VSDI orientation tuning curve was not
437 sensitive to the specific spatial filtration range (Fig. 6F, different line color).

438 Figures 7C and 7D (right columns) show the average tuning width and average normalized tuning
439 amplitude across all 8 VSDI experiments. As with the example experiment, the average VSDI tuning
440 width (σ=35.9°) is significantly larger than for single V1 neurons ($p=0.03$; t-test), while the average
441 normalized tuning amplitude is much smaller than for single V1 neurons ($p<0.001$; t-test). Figure 7E
442 shows the average normalized orientation tuning curves of VSDI and single V1 neurons, while Figure 7F
443 shows the average normalized tuning curves after removing the non-tuned response. Overall, the
444 average tuning curves of VSDI signals and single V1 neurons are dramatically different.

445

446 **Computational model of the relationship between VSDI signals and spiking activity of neural**
447 **populations**

448 Our results show large and systematic differences between the average tuning properties of single-unit
449 spiking activity and VSDI signals in V1. As discussed above, two factors are likely to contribute to these
450 differences. First, because membrane potential tends to be more broadly tuned and less selective than

spiking activity in single neurons, any contribution of subthreshold responses to VSDI signals will lead to broader and less selective VSDI responses. Second, the spatial integration area of VSDI signals could lead to broader and less selective VSDI responses.

To understand how these two factors are expected to influence the tuning properties of VSDI signals, we developed a simple computational model that describes the relationship between spiking activity of neural populations and VSDI signals in V1. The model, which is illustrated schematically in Figure 8, starts with the average spiking activity tuning curves of single V1 neurons (Fig. 8A), and ends with the predicted average VSDI tuning curves (Fig. 8E). It takes into account the structure of the V1 topographic maps for space and orientation (Fig. 8C). Finally, the model allows one to vary parametrically (as described below) the assumptions regarding the relative contribution of sub- and supra-threshold responses to VSDI signals (Fig. 8B), and the VSDI integration area (Fig. 8D), and to examine how these two factors influence the predicted average VSDI tuning properties.

We start by considering the expected effect of the relative contribution of spikes vs. subthreshold responses to VSDI signals. Intracellular recording experiments have demonstrated that the relationship between average membrane potential and firing rate in individual cortical neurons can be described by a power law of the form:

$$(1) \quad R_{SU} = k[V_m - V_0]_+^N$$

where R_{SU} is the average firing rate in a short temporal interval, k is a constant, V_m is the average membrane potential, V_0 is the average membrane potential below which the neuron does not spike, $[\ ]_+$ represents rectification and N is an exponent (typically in the range of 3-4 for single V1 neurons)((Anderson, Lampl et al. 2000; Priebe, Mechler et al. 2004). This relationship provides a

472 convenient way to model the contribution of spikes vs. subthreshold responses to VSDI signals. Thus, in
473 our model, the transfer function that relates average firing rate and average VSDI signal is given by:

474 (2) $$R_{SU} = k(R_{VSDI})^N$$

475 where R_{VSDI} is the average normalized VSDI signal. In other words, the model assumes that the average
476 firing rate of a population of neurons in a short temporal interval is proportional to the average VSDI
477 signal in the corresponding region to the power of *N*. If the VSDI signal reflected only spikes, the
478 relationship between the VSDI signal and spiking activity would be linear (Fig. 8B, *N=1*). If, on the other
479 hand, the VSDI signal reflected only subthreshold membrane potential, the relationship of the VSDI
480 signal to spiking activity would match the average relationship between membrane potential and spikes
481 in single neurons (Fig. 8B, *N=~4*). Different relative contributions of spiking vs. subthreshold responses
482 to the VSDI signal can therefore be approximated by the exponent *N* of the power function, which is the
483 first of the two free parameters of our model.

484 To see how this relative contribution is expected to affect the tuning properties of VSDI responses,
485 Figure 9A (top) shows the expected width of the VSDI position tuning curve for different values of the
486 exponent of the VSDI-to-spikes transfer function. As the exponent increases from 1 (i.e., dominant
487 spikes) to 4 (i.e., dominant subthreshold synaptic activity), the expected VSDI position tuning curve
488 becomes wider. Specifically, for an exponent *N=4*, the expected VSDI position tuning curve is twice as
489 wide as the curve for spiking activity, as observed in our VSDI measurements (Fig. 3A).

490 Similarly, as the exponent *N* increases from 1 to 4, the predicted VSDI orientation tuning amplitude
491 drops (Fig. 9A, middle panel), but even for a value of 4, the predicted orientation tuning amplitude is
492 much higher than the observed VSDI tuning amplitude. Finally, to better examine the orientation tuning
493 width, the bottom panel in Fig. 9A shows the normalized orientation tuning curves after the untuned

494 response has been removed. As the exponent *N* increases from 1 to 4, the predicted VSDI orientation
495 tuning curve becomes wider (Fig. 9A, bottom panel), but it remains far narrower than the observed VSDI
496 orientation tuning curve. The exponent has a weaker effect on orientation tuning width than on position
497 tuning width because the average orientation tuning curve of single V1 neurons has a significant
498 untuned component (Fig. 8E). These results show that, while a dominant contribution of subthreshold
499 responses to VSDI signals could account for the observed VSDI position tuning curve (Fig. 9A, top panel),
500 it is insufficient, by itself, to account for the observed VSDI orientation tuning curve (Fig. 9A, middle and
501 bottom panels).

502 We next consider the effect of the VSDI integration area. Two factors contribute to the size of this area.
503 First, due to light scattering properties of cortical tissue and blurring introduced by the optics, some of
504 the fluorescent signal arriving to the camera at a given pixel originates from cortical locations
505 corresponding to nearby pixels. Computational analysis (Polimeni, Granquist-Fraser et al. 2005) and
506 experimental measurements (Petersen, Grinvald et al. 2003) suggest that this spread has a space
507 constant of around 0.1 mm. A second, and probably more dominant, contribution comes from the
508 horizontal spread of dendrites and axons in the cortex (e.g., (Lund 1988)).

509 To capture the effect of the VSDI integration area on the tuning of VSDI responses, we modeled the VSDI
510 signals at a given location as the sum of responses of a population of nearby neurons, weighted by a 2-D
511 Gaussian with a space constant σ_{Int} centered at that location (as in (Katzner, Nauhaus et al. 2009)).
512 Therefore, the second free parameter of our model is the space constant σ_{Int}. We start by examining the
513 effect of the VSDI integration area in isolation, initially ignoring the possible contribution of
514 subthreshold responses to VSDI signals (i.e., assuming that *N*=1). We later combine these two factors.

515 To estimate the expected VSDI tuning curve for a given stimulus feature, say orientation, as a function of
516 σ_{Int}, we first computed the expected spatial pattern of spiking responses to each stimulus orientation. To

517 do this, we applied the average single-unit orientation tuning curve at each location, adjusting the
518 preferred orientation based on the corresponding orientation map (Fig. 8C). The spiking response to a
519 given stimulus orientation at each location was assumed to depend only on the difference between
520 stimulus orientation and the preferred orientation at this location. To obtain the expected pattern of
521 VSDI response following spatial integration, we applied the Gaussian weights at each location, assuming
522 a particular value for σ_{Int} (Fig. 8D). By combining the predicted responses to all stimulus orientations, we
523 obtained an orientation tuning curve at each location. Finally, we aligned the tuning curves to peak at
524 zero and averaged across all locations to obtain the predicted VSDI orientation tuning curve (Fig. 8E).

525 Before examining the effect of the VSDI integration area, we investigated more quantitatively the spatial
526 scales of the position and orientation maps in macaque V1. Because VSDI signals at each location
527 represent the integrated activity across a population of neurons, and because the preferred parameter
528 of V1 neurons changes systematically across the cortical surface, VSDI signals from each location receive
529 contributions from neurons with different preferred parameters. This spatial integration, or blurring, is
530 expected to lead to changes in the tuning properties of the VSDI signals relative to the average tuning of
531 individual V1 neurons. The extent to which a given integration area will affect the relative tuning of VSDI
532 responses and SU activity, depends on the rate at which the preferred parameter changes across the
533 cortical surface. This rate can be characterized by a length constant λ_{map} (in mm), which is equal to the
534 average horizontal distance that one has to travel in order for the preferred parameter (either
535 orientation or position) to shift by one tuning width.

536 To estimate $\lambda_{position}$, we computed from our position tuning VSDI measurements the average slope of the
537 curve that relates distance in visual space to distance in the cortex (Fig. 10A). This slope is equal to the
538 average cortical magnification factor at eccentricities of 1.8-3.4 (3.8 mm/°). We then estimated $\lambda_{position}$
539 as the cortical distance that corresponds to the average SU position tuning width and obtained a value

of 0.95 mm. Recent results from our laboratory indicate that $\lambda_{position}$, which is related to the size of the cortical point image (McIlwain 1986), is invariant with eccentricity in parafoveal V1 (Palmer, Chen et al. 2012).

To estimate $\lambda_{orientation}$, we computed the average difference in preferred orientation between all pairs of points in our orientation maps, as a function of their cortical distance (Fig. 10B). We then estimated $\lambda_{orientation}$ as the cortical distance that corresponds to the average SU orientation tuning width. In the case of the orientation map, $\lambda_{orientation}$ is ~0.12 mm (Fig. 10B), almost an order of magnitude smaller than $\lambda_{position}$. Therefore, a VSDI integration area of σ_{Int} = 0.2 mm will cause neurons with very different preferred orientations to contribute to VSDI responses at a given location, while the same integration area will cause neurons with nearly identical position tuning curves to contribute to VSDI responses at the same location.

These results suggest that the average VSDI orientation tuning curve should be strongly affected by spatial integration areas with σ_{Int} in the range of 0.1-0.3 mm, while the average VSDI spatial tuning curve should be nearly invariant to integration areas within this range. Consistent with these predictions, the VSDI integration area has a large impact on the predicted VSDI orientation tuning curve (Figs. 9B, middle and bottom panels) but has negligible impact on the predicted VSDI position tuning curve (Fig. 9B, top panel). Specifically, increasing σ_{Int} from 0.1 mm to 0.3 mm leads to a large broadening of the predicted VSDI orientation tuning curve and a large reduction in the VSDI orientation tuning amplitude, but even an integration area with σ_{Int} of 0.3 mm is not sufficient to account for the observed VSDI orientation tuning curve.

So far we considered the effects of the VSDI integration area and the relative contribution of spikes vs. subthreshold responses to VSDI signals separately. To consider the combined effect of both factors, we performed a bootstrap analysis on our experimental results (see Methods), estimating simultaneously

563 the two free parameters, N and σ_{Int}. We applied this analysis independently to our orientation and
564 position tuning data. The results are shown in Table 1. Across the two stimulus dimensions, VSDI tuning
565 curves are consistent with an exponent that is close to 4. These results suggest that VSDI signals are
566 dominated by subthreshold synaptic activity. In addition, the analysis shows that the VSDI orientation
567 tuning curves are consistent with a VSDI integration area with σ_{Int} of ~230 µm. As discussed above,
568 because the spatial scale of the retinotopic map is much larger than the VSDI integration area, our
569 position tuning results do not constrain the estimate of the VSDI integration area but provide a highly
570 constrained estimate of the power function exponent. Figure 9C shows that, using N = 3.8 and σ_{Int}
571 between 200 and 300 µm, the predicted VSDI tuning properties are consistent with the observed ones.

572

573 **Discussion**

574 The goal of the current study was to address two fundamental questions regarding the nature of VSDI
575 signals and their relation to the average spiking activity of local populations of cortical neurons. To
576 address these questions, we developed a simple computational model that allows one to predict the
577 tuning properties of VSDI signals from the average tuning properties of single cortical neurons and from
578 the underlying functional maps. To constrain this model, we measured VSDI signals and spiking activity
579 of single neurons from V1 of behaving monkeys and compared the tuning properties of these two
580 signals across two stimulus dimensions: orientation and spatial position. Our results suggest that VSDI
581 signals in the cortex are dominated by subthreshold synaptic activity and receive little contribution from
582 spiking activity. In addition, our results suggest that VSDI signals at a given cortical location are equal to
583 a weighted sum of neural responses at neighboring locations, with Gaussian weights with radius (σ_{Int}) of
584 ~230 µm centered at that location. These results help interpret a large body of work that used VSDI to
585 measure neural population responses in the cortex *in vivo* (e.g.,(Grinvald, Lieke et al. 1994; Arieli, Sterkin

586 et al. 1996; Tsodyks, Kenet et al. 1999; Seidemann, Arieli et al. 2002; Sharon and Grinvald 2002; Slovin,
587 Arieli et al. 2002; Kenet, Bibitchkov et al. 2003; Petersen, Grinvald et al. 2003; Jancke, Chavane et al.
588 2004; Chen, Geisler et al. 2006; Benucci, Frazor et al. 2007; Yang, Heeger et al. 2007; Chen, Geisler et al.
589 2008; Sit, Chen et al. 2009; Huang, Xu et al. 2010) , for review see (Grinvald and Hildesheim 2004)). In
590 addition, our findings could help in designing future VSDI experiments.

591 We found that VSDI signals are substantially less selective than the average spiking activity of single V1
592 neurons across the two stimulus dimensions. The difference in position tuning width between VSDI
593 signals and single-unit spiking activity is comparable to differences between receptive field size of
594 subthreshold and suprathreshold responses in individual V1 neurons (e.g., (Bringuier, Chavane et al.
595 1999; Nowak, Sanchez-Vives et al. 2010)). With respect to orientation tuning, VSDI signals are more
596 broadly tuned and contain a much larger untuned component than spiking activity of single V1 neurons.
597 While membrane potential in single V1 neurons is also more broadly tuned and contains a larger
598 untuned component than spiking activity (for review, see (Priebe and Ferster 2008)), VSDI signals are
599 substantially less orientation selective than single-unit membrane potentials. The additional reduction in
600 orientation selectivity of VSDI signals relative to membrane potential of single neurons can be attributed
601 to the spatial integration of VSDI, which combines neural signals from a population of neurons with
602 different preferred orientations at each cortical location.

603 Our results suggest that the VSDI integration area has a radius (σ_{Int}) of ~230 µm. Recent studies used a
604 similar approach to estimate the integration area of local field potentials (LFP)(Katzner, Nauhaus et al.
605 2009; Xing, Yeh et al. 2009). While the results of Katzner et al. (2009) suggest that the LFP signals have
606 an integration radius of less than 100 µm and are therefore substantially more local than the VSDI
607 signals, the results of Xing et al. (2009) suggest that the LFP integration radius is comparable to that of

608 the VSDI signals. Additional studies are necessary to better understand the relationship between the
609 VSDI and LFP signals.

610 Our results show that the relationship between VSDI signals and spiking activity is well captured by a
611 power function with an exponent of ~4. Similar power functions with comparable exponents are
612 obtained when examining the relationship between average membrane potential and average spike rate
613 in single V1 neurons (Anderson, Lampl et al. 2000; Priebe, Mechler et al. 2004). Several studies,
614 however, have demonstrated that the relationship between membrane potential and spike rate in single
615 neurons depends on stimulus contrast ((Anderson, Lampl et al. 2000); reviewed in (Priebe and Ferster
616 2008)). Specifically, for SUs, the exponent of the power function tends to decrease at low contrast,
617 consistent with an increase in response gain at low contrast. Therefore, one would predict a similar
618 change with contrast in the power function that relates VSDI signals to spiking activity. Previous results
619 regarding the spatial spread of SU responses and VSDI signals are consistent with this prediction.
620 Specifically, our previous work demonstrated that the spatial spread of VSDI responses to a small
621 oriented stimulus is largely invariant to stimulus contrast (Chen, Geisler et al. 2006; Chen, Geisler et al.
622 2008; Sit, Chen et al. 2009). In contrast, multiple studies have demonstrated that the size of the
623 suprathreshold receptive field of single V1 neurons increases substantially at low-contrast relative to
624 high contrast (e.g., (Sceniak, Ringach et al. 1999; Cavanaugh, Bair et al. 2002)). These results imply that
625 the difference in response spread between VSDI signals and spiking activity is likely to become smaller at
626 lower contrast, consistent with a reduction in the exponent of the power function that relates VSDI
627 signals to spiking activity.

628 VSDI is a powerful technique that allows one to measure neural population responses simultaneously
629 over large cortical regions with millisecond temporal resolution. The integration area of VSDI reported
630 here affects its spatial resolution. However, it is important to note that the integration area does not

imply an inability of this technique to resolve neural signals at a much finer spatial scale. Our previous study of the retinotopic map in macaque V1 (Yang, Heeger et al. 2007) and the detailed orientation maps reported here (Fig. 6) demonstrate that one can use VSDI in behaving animals to resolve neural responses that vary at a spatial scale of ~100 µm.

VSDI has several advantages over multi-electrode electrophysiological techniques as a tool for measuring neural population responses. First, in contrast to the sparse sampling afforded by electrode arrays, VSDI provides a complete and dense coverage of the imaged area. Second, in contrast to the rigid nature of electrode arrays, the field-of-view of VSDI and the pixel size can be easily adjusted by changing the lens combination on the imaging camera, therefore providing high flexibility in studying responses from an entire population of neurons over regions from several mm^2 to several cm^2. A major limitation of VSDI has been the lack of understanding of the relationship between VSDI signals and neural population responses at the spiking activity level. The current study provides a first step in addressing this important question.

Our finding that the same model parameters can account for the differences between tuning properties of VSDI and SU spiking activity across two different stimulus dimensions (position and orientation) raises the possibility that, across a range of stimulus parameters, one could use our computational model and estimated model parameters to predict the average pattern of population responses at the spiking level from the VSDI signals, and vice versa. To illustrate the potential of this approach, Figure 11 shows a 1-D slice through a simulated pattern of VSDI signals in response to a small oriented Gabor patch (black curve). Using our model, we can remove the effect of VSDI spatial integration (by de-convolving the VSDI signals with the proper kernel) to obtain the predicted pattern of neural responses at the level of membrane potentials (dark gray curve). In comparison to the VSDI signals, the predicted response at the level of membrane potential has a substantially smaller orientation untuned component but a similar

spatial extent. Finally, by applying the inverse of the power function describing the relation between VSDI signals and spiking activity, we obtain an estimate of the population response at the spiking level (light gray curve). This step leads to a substantial reduction in the spread of the population response, and an additional decrease in the orientation untuned component of the population response relative to the VSDI signals. This analysis demonstrates the potential utility of applying this model to VSDI signals. An important goal for future experiments is therefore to test the validity of this model for other stimulus dimensions in V1, and for other cortical areas where information is organized topographically.

ACKNOWLEDGEMENTS

We thank C. Michelson, M. Michel and N. Priebe for discussions and T. Cakic for technical support.

Present addresses: C. R. Palmer, Division of Biological Sciences at University of California at San Diego; Y. Chen, Dept. of Psychology and Center for Perceptual Systems at University of Texas at Austin; E. Seidemann, Dept. of Psychology and Center for Perceptual Systems at University of Texas at Austin.

GRANTS

This work was supported by National Eye Institute grants EY-016454 and EY-016752.

DISCLOSURES

No conflicts of interest, financial or otherwise, are declared by the authors.

673 **References**

674

675 Adams, D. L. and J. C. Horton (2003). "A precise retinotopic map of primate striate cortex generated
676 from the representation of angioscotomas." Journal of Neuroscience **23**(9): 3771-3789.
677 Anderson, J. S., I. Lampl, et al. (2000). "The contribution of noise to contrast invariance of orientation
678 tuning in cat visual cortex." Science **290**(5498): 1968-1972.
679 Arieli, A. and A. Grinvald (2002). "Optical imaging combined with targeted electrical recordings,
680 microstimulation, or tracer injections." Journal of Neuroscience Methods **116**(1): 15-28.
681 Arieli, A., A. Grinvald, et al. (2002). "Dural substitute for long-term imaging of cortical activity in
682 behaving monkeys and its clinical implications." Journal of Neuroscience Methods **114**(2): 119-
683 133.
684 Arieli, A., A. Sterkin, et al. (1996). "Dynamics of ongoing activity: Explanation of the large variability in
685 evoked cortical responses." Science **273**(5283): 1868-1871.
686 Benucci, A., R. A. Frazor, et al. (2007). "Standing waves and traveling waves distinguish two circuits in
687 visual cortex." Neuron **55**(1): 103-117.
688 Blasdel, G. G. and G. Salama (1986). "Voltage-Sensitive Dyes Reveal a Modular Organization in Monkey
689 Striate Cortex." Nature **321**(6070): 579-585.
690 Bonhoeffer, T. and A. Grinvald (1991). "Iso-Orientation Domains in Cat Visual-Cortex Are Arranged in
691 Pinwheel-Like Patterns." Nature **353**(6343): 429-431.
692 Bringuier, V., F. Chavane, et al. (1999). "Horizontal Propagation of Visual Activity in the Synaptic
693 Integration Field of Area 17 Neurons." Science **283**(5402): 695-699.
694 Cavanaugh, J. R., W. Bair, et al. (2002). "Nature and interaction of signals from the receptive field center
695 and surround in macaque V1 neurons." Journal of Neurophysiology **88**(5): 2530-2546.
696 Chen, Y., W. S. Geisler, et al. (2006). "Optimal decoding of correlated neural population responses in the
697 primate visual cortex." Nat Neurosci **9**(11): 1412-1420.
698 Chen, Y., W. S. Geisler, et al. (2008). "Optimal Temporal Decoding of V1 Population Responses in a
699 Reaction-Time Detection Task." J Neurophysiol **99**(3): 1366-1379.
700 Daniel, P. M. and D. Whitteridge (1961). "The representation of the visual field on the cerebral cortex in
701 monkeys." J Physiol. **159** (2): 203-221.
702 Devalois, R. L., E. W. Yund, et al. (1982). "THE ORIENTATION AND DIRECTION SELECTIVITY OF CELLS IN
703 MACAQUE VISUAL-CORTEX." Vision Research **22**(5): 531-544.
704 Grinvald, A. and R. Hildesheim (2004). "VSDI: A new era in functional imaging of cortical dynamics."
705 Nature Reviews Neuroscience **5**(11): 874-885.
706 Grinvald, A., E. E. Lieke, et al. (1994). "Cortical Point-Spread Function and Long-Range Lateral
707 Interactions Revealed by Real-Time Optical Imaging of Macaque Monkey Primary Visual-Cortex."
708 Journal of Neuroscience **14**(5): 2545-2568.
709 Huang, X., W. Xu, et al. (2010). "Spiral Wave Dynamics in Neocortex." Neuron **68**(5): 978-990.
710 Hubel, D. H. and T. N. Wiesel (1963). "Shape and arrangement of columns in cat's striate cortex." Journal
711 of Physiology **165**(1): 559-568.
712 Hubel, D. H. and T. N. Wiesel (1968). "Receptive fields and functional architecture of monkey striate
713 cortex." Journal of Physiology **195**(1): 215-243.
714 Hubel, D. H. and T. N. Wiesel (1974). "Uniformity of monkey striate cortex: a parallel relationship
715 between field size, scatter and magnification factor." J Comp Neurol **158**: 295-306.
716 Jancke, D., F. Chavane, et al. (2004). "Imaging cortical correlates of illusion in early visual cortex." Nature
717 **428**(6981): 423-426.
718 Katzner, S., I. Nauhaus, et al. (2009). "Local Origin of Field Potentials in Visual Cortex." Neuron **61**(1): 35-
719 41.

720 Kenet, T., D. Bibitchkov, et al. (2003). "Spontaneously emerging cortical representations of visual
721 attributes." Nature **425**(6961): 954-956.
722 Levitt, J. B. and J. S. Lund (2002). "The spatial extent over which neurons in macaque striate cortex pool
723 visual signals." Vis Neurosci **19**(4): 439-452.
724 Lund, J. S. (1988). "Anatomical Organization of Macaque Monkey Striate Visual Cortex." Ann. Rev.
725 Neurosci. **11**(1): 253-288.
726 McIlwain, J. T. (1986). "Point images in the visual system: new interest in an old idea." Trends in
727 Neurosci. **9**: 354-358.
728 Mountcastle, V. B. (1957). "Modality and topographic properties of single neurons of cat's somatic
729 sensory cortex." Journal Of Neurophysiology **20**(4): 408-434.
730 Nauhaus, I., A. Benucci, et al. (2008). "Neuronal selectivity and local map structure in visual cortex."
731 Neuron **57**(5): 673-679.
732 Nienborg, H. and B. G. Cumming (2006). "Macaque V2 neurons, but not V1 neurons, show choice-
733 related activity." Journal of Neuroscience **26**(37): 9567-9578.
734 Nowak, L. G., M. V. Sanchez-Vives, et al. (2010). "Spatial and Temporal Features of Synaptic to Discharge
735 Receptive Field Transformation in Cat Area 17." Journal of Neurophysiology **103**(2): 677-697.
736 Obermayer, K. and G. G. Blasdel (1993). "Geometry of Orientation and Ocular Dominance Columns in
737 Monkey Striate Cortex." Journal of Neuroscience **13**(10): 4114-4129.
738 Palmer, C., S.-Y. Cheng, et al. (2007). "Linking Neuronal and Behavioral Performance in a Reaction-Time
739 Visual Detection Task." J Neurosci **27**(30): 8122-8137.
740 Palmer, C. R., Y. Chen, et al. (2012). "Uniform spatial spread of population activity in primate parafoveal
741 V1." J Neurophysiol **(in press)**.
742 Petersen, C. C. H., A. Grinvald, et al. (2003). "Spatiotemporal dynamics of sensory responses in layer 2/3
743 of rat barrel cortex measured in vivo by voltage-sensitive dye imaging combined with whole-cell
744 voltage recordings and neuron reconstructions." Journal of Neuroscience **23**(4): 1298-1309.
745 Polimeni, J. R., D. Granquist-Fraser, et al. (2005). "Physical limits to spatial resolution of optical
746 recording: Clarifying the spatial structure of cortical hypercolumns." Proceedings of the National
747 Academy of Sciences of the United States of America **102**(11): 4158-4163.
748 Priebe, N. J. and D. Ferster (2008). "Inhibition, spike threshold, and stimulus selectivity in primary visual
749 cortex." Neuron **57**(4): 482-497.
750 Priebe, N. J., F. Mechler, et al. (2004). "The contribution of spike threshold to the dichotomy of cortical
751 simple and complex cells." Nat Neurosci **7**(10): 1113-1122.
752 Read, J. C. A. and B. G. Cumming (2003). "Measuring V1 receptive fields despite eye movements in
753 awake monkeys." Journal of Neurophysiology **90**(2): 946-960.
754 Salzberg, B. M., H. V. Davila, et al. (1973). "Optical recording of impulses in individual neurones of an
755 invertebrate central nervous system." Nature **246**(5434): 508-509.
756 Sceniak, M. P., D. L. Ringach, et al. (1999). "Contrast's effect on spatial summation by macaque V1
757 neurons." Nat Neurosci **2**(8): 733-739.
758 Seidemann, E., A. Arieli, et al. (2002). "Dynamics of depolarization and hyperpolarization in the frontal
759 cortex and saccade goal." Science **295**(5556): 862-865.
760 Sharon, D. and A. Grinvald (2002). "Dynamics and constancy in cortical spatiotemporal patterns of
761 orientation processing." Science **295**(5554): 512-515.
762 Shoham, D., D. E. Glaser, et al. (1999). "Imaging cortical dynamics at high spatial and temporal resolution
763 with novel blue voltage-sensitive dyes." Neuron **24**(4): 791-802.
764 Sit, Y.-F., Y. Chen, et al. (2009). "Complex dynamics of V1 population responses explained by a simple
765 gain-control model." Neuron **24**(64(6)): 943-956.
766 Slovin, H., A. Arieli, et al. (2002). "Long-term voltage-sensitive dye imaging reveals cortical dynamics in
767 behaving monkeys." Journal of Neurophysiology **88**(6): 3421-3438.

768 Talbot, S. A. and W. H. Marshall (1941). "Physiological studies on neural mechanisms of visual
769 localization and discrimination." Am J Ophthalmol **24**: 1255-1264.
770 Tootell, R. B. H., M. S. Silverman, et al. (1982). "Deoxyglucose Analysis of Retinotopic Organization in
771 Primate Striate Cortex." Science **218**(4575): 902-904.
772 Tootell, R. B. H., E. Switkes, et al. (1988). "Functional-Anatomy of Macaque Striate Cortex .2. Retinotopic
773 Organization." Journal of Neuroscience **8**(5): 1531-1568.
774 Tso, D. Y., R. D. Frostig, et al. (1990). "Functional-Organization of Primate Visual-Cortex Revealed by
775 High-Resolution Optical Imaging." Science **249**(4967): 417-420.
776 Tsodyks, M., T. Kenet, et al. (1999). "Linking spontaneous activity of single cortical neurons and the
777 underlying functional architecture." Science **286**(5446): 1943-1946.
778 Van Essen, D. C., W. T. Newsome, et al. (1984). "The visual field representation in striate cortex of the
779 macaque monkey: Asymmetries, anisotropies, and individual variability." Vis. Res. **24**(5): 429-
780 448.
781 Vogels, R. and G. A. Orban (1990). "How well do response changes of striate neurons signal differences
782 in orientation: a study in the discriminating monkey." J Neurosci **10**(11): 3543-3558.
783 Woolsey, C. N. (1952). Patterns of localization in sensory and motor areas of the cerebral cortex. The
784 Biology of Mental Health and Disease. New York, Hoeber**:** 193-206.
785 Xing, D., C.-I. Yeh, et al. (2009). "Spatial Spread of the Local Field Potential and its Laminar Variation in
786 Visual Cortex." J. Neurosci. **29**(37): 11540-11549.
787 Yang, Z., D. J. Heeger, et al. (2007). "Rapid and precise retinotopic mapping of the visual cortex obtained
788 by voltage sensitive dye imaging in the behaving monkey." J Neurophysiol **98**(2): 1002-1014.

789

790

791

792 **Table 1: Estimated model parameters**

	Power function exponent *N*	Integration area σ
Position tuning	3.9±1.0	--
Orientation tuning	3.8±1.0	233±36 μm

793

794

795 ## Figure legends

796 **Figure 1** Position tuning properties of an example V1 neuron. (A) Stimulus position. Fixation point is at
797 the origin. Circles indicate stimulus positions with circle radius equal to stimulus σ (0.167°) (B) PSTH of a
798 V1 neuron as the distance between stimulus center and RF center is varied. Shaded areas show periods
799 in which mean firing rate was computed. (C) Position tuning curve obtained from B. The solid curve
800 shows a 1-D half Gaussian fit. Estimated tuning width is indicated in the top right. Horizontal line shows
801 spontaneous activity ±SEM (shaded area). Error bars in all figures represent ±SEM.

802 **Figure 2** Example position tuning of VSDI signal. (A) Stimulus position. Same format as Fig. 1A. Colored
803 wedge shape shows the region in visual space that is approximately represented by the corresponding
804 rectangle area in B. (B) Image of cortical vasculature with the approximate retinotopic mapping. The
805 rectangle with four colors corresponds to the wedge-shaped area in A, while the elongated cyan
806 rectangle corresponds to the predicted trajectory of the stimuli along the cortical surface. (C) Spatial
807 distributions of response to stimuli at different positions. Responses were averaged during a 200 ms
808 interval starting 36 ms after stimulus onset. Ellipsoids show 1-σ contour of the 2-D Gaussian fit to the
809 response. Colored squares (0.75 x 0.75 mm^2) denote the center of the 2-D Gaussian functions. The
810 center position for the most foveal position (red) is shown in all panels for reference. All centers are
811 shown on the bottom right panel. (D) Position tuning curves for the 6 locations in C. The colors

812 represent different positions. The solid curve shows a 1-D Gaussian fit. Estimated tuning width is
813 indicated in each panel.

814 **Figure 3** Summary of position tuning width for single V1 neurons and for VSDI signals, and analysis of the
815 possible effect of variations in fixational eye position on position tuning width of single V1 neurons. (A)
816 Bar plot of average position tuning widths for SUs and VSDI. (B) Average normalized position tuning
817 curves. Shaded areas represent ±SEM. (C) For each SU we computed the standard deviation of eye
818 position (within trial) during stimulus presentation. The bar plot shows the mean position tuning widths
819 for SUs with below median (left) and above median (right) eye position SD. p value - one-tailed t-tests.
820 (D) Same format as C, but based on the standard deviation (across trials) of the mean eye position offset
821 from fixation point.

822 **Figure 4** Orientation tuning properties of an example V1 neuron. (A) PSTH of a V1 neuron responding to
823 a Gabor stimulus at 6 different orientations and in blank trials. Shaded areas show periods in which
824 mean firing rate was computed. Spontaneous firing rate was near zero. (B) Orientation tuning curve
825 obtained from A. The solid curve shows a 1-D circular Gaussian fit. Estimated normalized tuning
826 amplitude (NTA) and tuning width σ are indicated in the top right.

827 **Figure 5** Temporal dynamics of VSDI responses and signal-to-noise ratio (S/N) as a function of stimulus
828 frequency. Response to grating flashed at 2Hz (A) or 5Hz (B) was integrated over a cortical area of 1 x 1
829 mm^2 with pixel size of ~32 x 32 μm^2. Top: mean and SEM of time course of V1 responses averaged over
830 an area of 1x1 mm^2 in 6 separate experiments at each stimulus frequency. The mean response in blank
831 trials was subtracted from each trace. Middle: amplitude spectrum of the average evoked response
832 (solid) and average amplitude spectrum of the VSDI noise (dashed). The noise amplitude spectrum was
833 computed from the residual time courses (single-trial minus mean time course) and averaged across all
834 blank trials. Bottom: S/N computed as the d' or z-score from the middle panel. (C) Summary of average

835 S/N at stimulus frequency across experiments. The middle column indicates the average d' for 2 Hz
836 presentation when integrating the response over 200 ms, as in the analysis of the position tuning.

837 **Figure 6** Orientation tuning of VSDI signal. (A) Image of the cortical vasculature in the imaged area;
838 V1/V2 border is parallel to the top of the image. (B) Spatial 1-D power spectrum of the single-orientation
839 response maps. The 2-D power spectrum of each map was averaged radially and then averaged across
840 the 12 orientations. The peak at 1.2 cycle/mm is due to orientation columns with a corresponding peak
841 period of ~0.83 mm. (C) Average response maps to 4 out of 12 orientations. Only the components with
842 spatial frequency between 0.8 and 3 cycle/mm indicated by the shaded area between the dashed
843 vertical lines in (B) are shown. The spatial filtration removes components with periods larger than 1.25
844 mm and smaller than 0.33 mm. (D) Orientation map computed based on the vector sum of the
845 responses. Hue represents preferred orientation and saturation represents tuning amplitude. The white
846 square corresponds to the magnified region (0.7 x 0.7 mm^2) on the right. (E) Correlations between all
847 pairs of response maps as a function of the orientation difference. Different colors indicate different
848 range of spatial filtration. Adding lower or higher spatial frequencies cause the correlation functions to
849 flatten, suggesting that the added frequencies contribute components that are less orientation
850 selective. (F) Normalized VSDI orientation tuning curve including the untuned component. Different
851 colors indicate different range of spatial filtration. In E and F, SEMs are smaller than symbol.

852 **Figure 7** Average orientation tuning properties of SU and VSDI responses in V1. Histogram of tuning
853 width (A) and normalized tuning amplitude (B) for single V1 neurons. One unit was untuned (NTA~0;
854 σ~90°) and was removed from A. Bar histogram of average tuning widths (C) and average normalized
855 tuning amplitude (D) for SU and VSDI. (E) Average normalized orientation tuning curves for SU and VSDI
856 including the untuned response. Shaded area represents ±SEM. (F) Same as (E) but with untuned
857 responses removed.

858 **Figure 8** A schematic representation of our model of the relationship between average VSDI signals and
859 average spiking activity. (A) The model starts with the average SU tuning curve for position (left) and
860 orientation (right). (B) The local VSDI responses at each cortical location are obtained based on the
861 nonlinear relationship between average SU spiking activity and local VSDI signals. This relationship is
862 assumed to be consistent with a power law. The exponent *N* is one of the two free parameters of the
863 model. The figure shows three possible values for *N*: *N*=1 (linear relationship, consistent with VSDI being
864 dominated by spiking activity), *N*=4 (similar to the relationship between average membrane potential
865 and spike rate in single V1 neurons, consistent with VSDI being dominated by subthreshold membrane
866 potential), and *N*=2 (intermediate between the two extremes). (C) The predicted spatial pattern of VSDI
867 responses prior to spatial integration is computed based on the functional maps for position (retinotopy;
868 left) and orientation (right). The squares in each map represent a reference area of 1 x 1 mm^2. (D) To
869 model the effect of the VSDI spatial integration, the predicted VSDI response at each location is
870 computed as the weighted sum of the responses at neighboring locations, with Gaussian weights with a
871 space constant σ_{Int}. σ_{Int} is the 2nd free parameter of the model. Three values of σ_{Int} are indicated
872 schematically by the three Gaussians. Note that the size of the squares in D is 1 x 1 mm^2, the same as
873 the squares in C. The 1x1 mm^2 is small relative to the scale of the retinotopic map (C left) but large
874 relative to the scale of the orientation map (C, right). (E) Predicted average VSDI tuning curve for
875 position (left) and orientation (right) is obtained by aligning the predicted tuning curves from all
876 locations to peak at zero and averaging across locations.

877 **Figure 9** Model predictions. (A) Tuning curves for single units (dashed red), VSDI (dashed blue), and
878 predicted VSDI tuning curves based on the non-linear transfer function with three possible values of the
879 exponent *N* (solid curves). Top – position tuning; middle – orientation tuning with the untuned
880 response; bottom – orientation tuning with the untuned response removed. (B) Same as A, but showing
881 predicted VSDI tuning functions for three different values of the VSDI integration area. (C) Same as B,

882 but showing predicted VSDI tuning curves after assuming that VSDI signals are dominated by
883 subthreshold responses (*N*=3.8) while varying the VSDI integration area.

884 **Figure 10** Change in preferred parameters as a function of cortical distance for position (A) and
885 orientation (B) in macaque V1. Note that in A the y axis is in degrees of visual angle while in B it is in
886 degrees of polar angle. The dashed horizontal line indicates the corresponding average tuning width of
887 V1 neurons, while the dashed vertical line indicates the corresponding cortical distance λ which is the
888 length constant of each map.

889 **Figure 11** A synthetic example illustrating how our model could be used to predict V1 population
890 responses at the spiking activity level from the measured VSDI responses. Simulated 1-D slice through
891 VSDI responses to an oriented Gabor stimulus centered at position zero at the preferred orientation for
892 that location (black curve). The cortical response has two components – a large Gaussian envelope
893 component representing the contrast envelope of the Gabor stimulus (σ=1.5 mm), and a higher spatial
894 frequency pattern representing the cortical columns (~1.2 cycles/mm). The predicted pattern of
895 responses prior to the spatial integration can be obtained by de-blurring the VSDI response with the
896 proper kernel (dark gray curve). Note that the overall width of the response remains the same but the
897 magnitude of the modulations at the columnar scale increases several fold. The predicted pattern at the
898 level of spiking activity (light gray curve) can be obtained by applying the inverse of the non-linear
899 transfer function relating VSDI signals to spiking activity. Note that the response spread is reduced by a
900 factor of 2 and the modulations at the columnar scale increase even further.

901

Fig 1

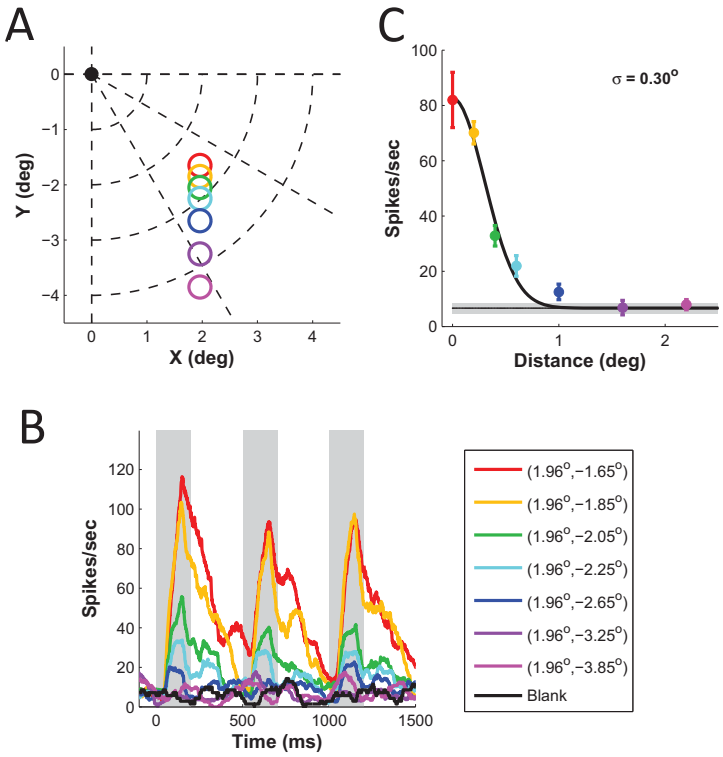
A
Y (deg)
X (deg)
C
σ = 0.30°
Spikes/sec
Distance (deg)
B
Spikes/sec
Time (ms)
(1.96°,−1.65°)
(1.96°,−1.85°)
(1.96°,−2.05°)
(1.96°,−2.25°)
(1.96°,−2.65°)
(1.96°,−3.25°)
(1.96°,−3.85°)
Blank

Fig. 2

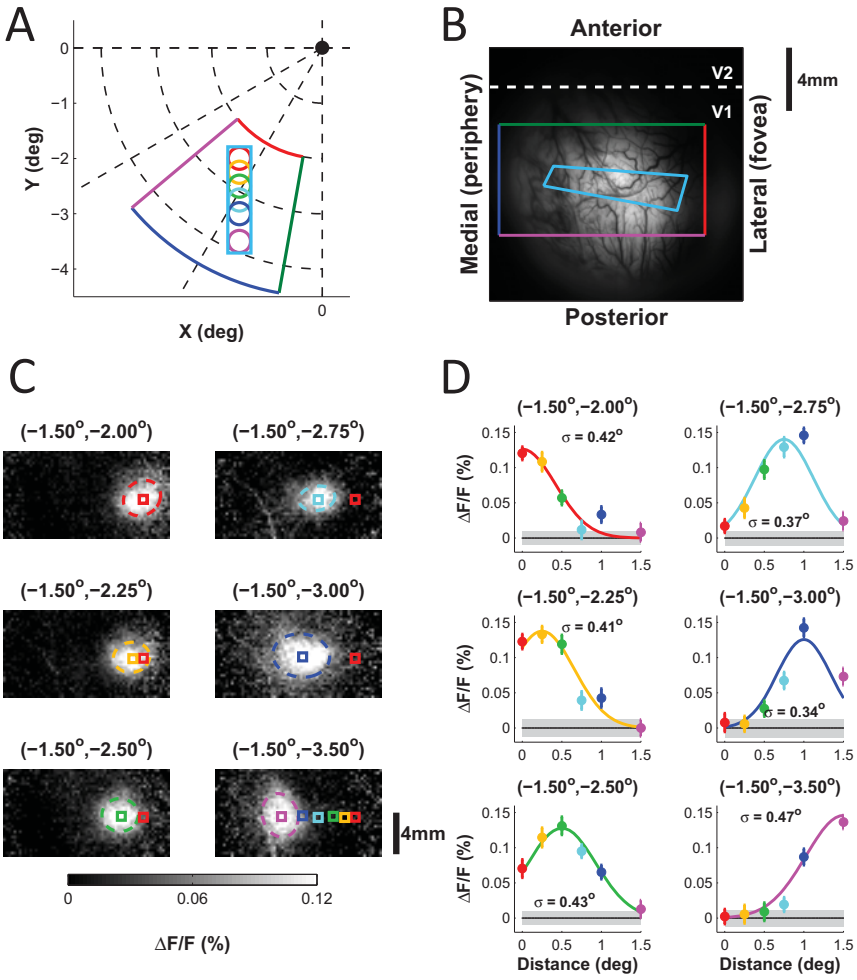
A
Y (deg)
X (deg)
B
Anterior
Posterior
Medial (periphery)
Lateral (fovea)
V2
V1
4mm
C
(−1.50°,−2.00°)
(−1.50°,−2.75°)
(−1.50°,−2.25°)
(−1.50°,−3.00°)
(−1.50°,−2.50°)
(−1.50°,−3.50°)
4mm
0
0.06
0.12
ΔF/F (%)
D
σ = 0.42°
σ = 0.37°
σ = 0.41°
σ = 0.34°
σ = 0.43°
σ = 0.47°
ΔF/F (%)
Distance (deg)

Fig. 3

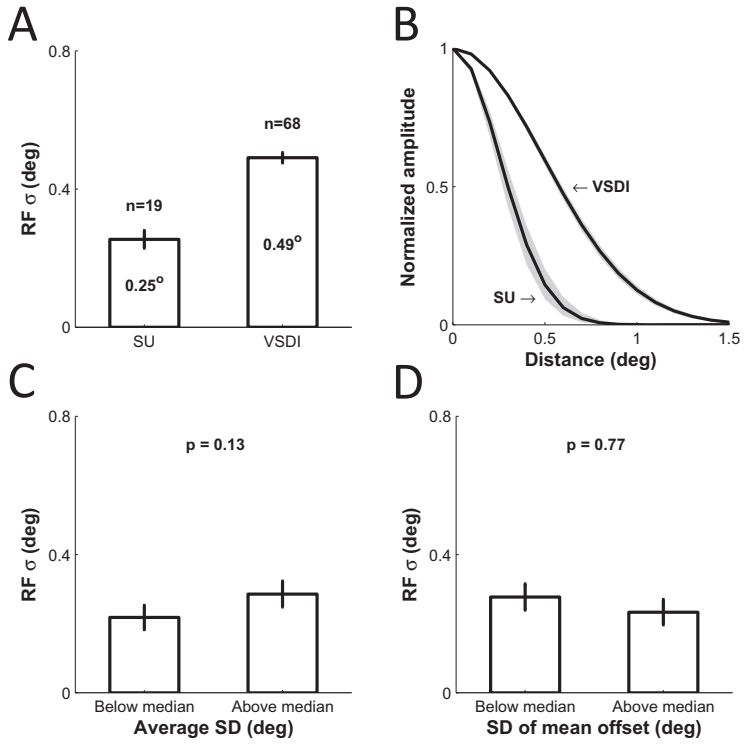
A
0.8
0.4
0
RF σ (deg)
n=19
n=68
0.25°
0.49°
SU
VSDI
B
1
0.5
0
Normalized amplitude
← VSDI
SU →
0
0.5
1
1.5
Distance (deg)
C
0.8
0.4
0
RF σ (deg)
p = 0.13
Below median
Above median
Average SD (deg)
D
0.8
0.4
0
RF σ (deg)
p = 0.77
Below median
Above median
SD of mean offset (deg)

Fig. 4

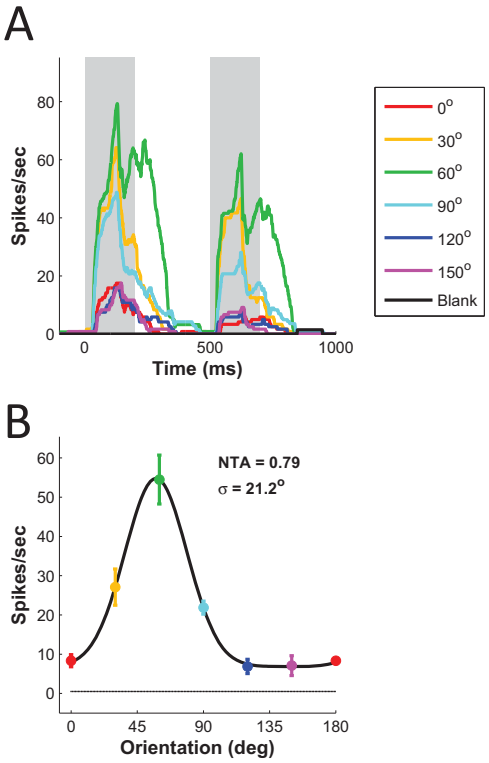
A
Spikes/sec
80
60
40
20
0
0
500
1000
Time (ms)
0°
30°
60°
90°
120°
150°
Blank
B
Spikes/sec
60
50
40
30
20
10
0
NTA = 0.79
σ = 21.2°
0
45
90
135
180
Orientation (deg)

Fig. 5

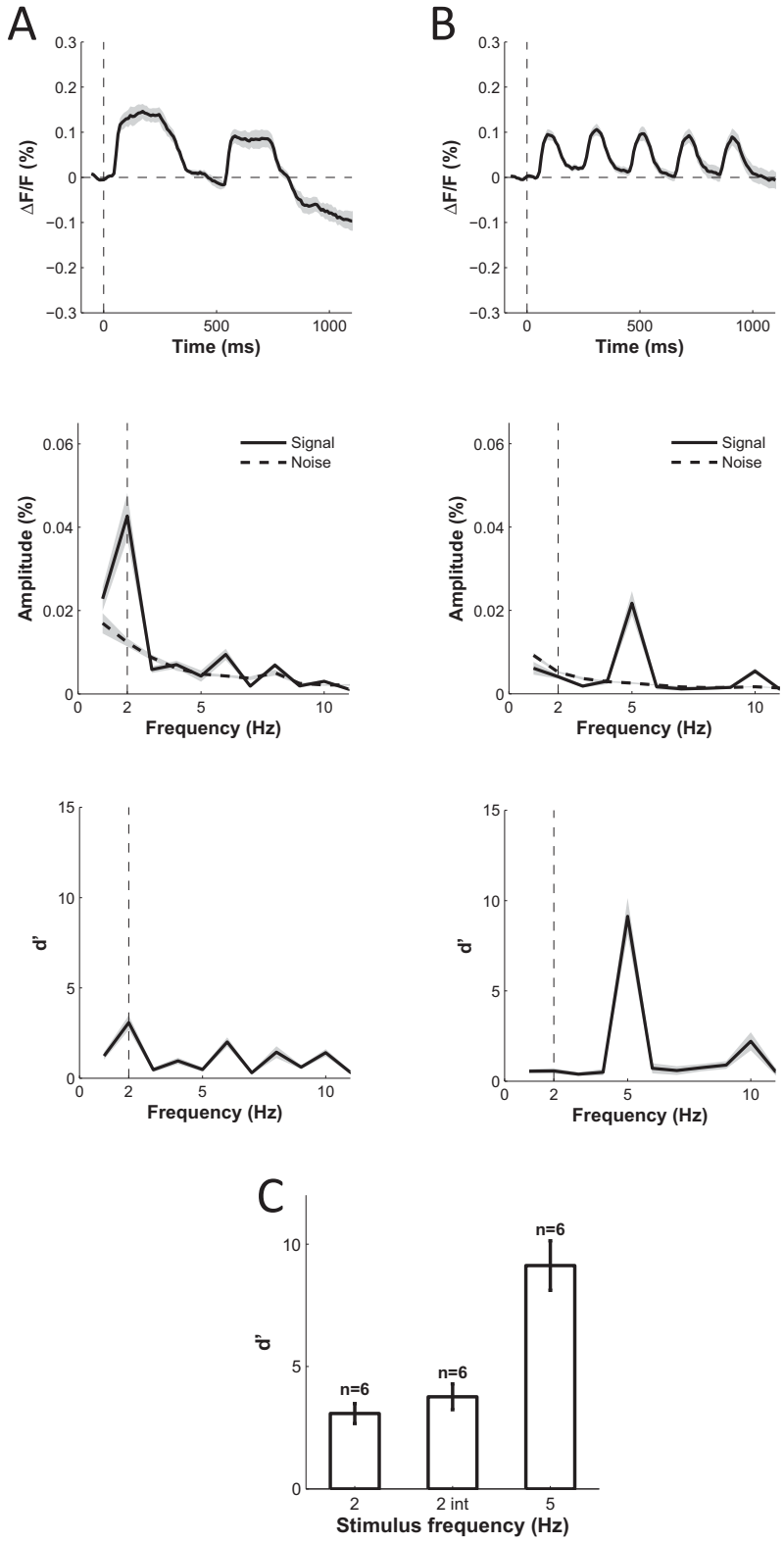
A
B
ΔF/F (%)
Time (ms)
Amplitude (%)
Signal
Noise
Frequency (Hz)
d'
C
n=6
2
2 int
5
Stimulus frequency (Hz)

Fig. 6

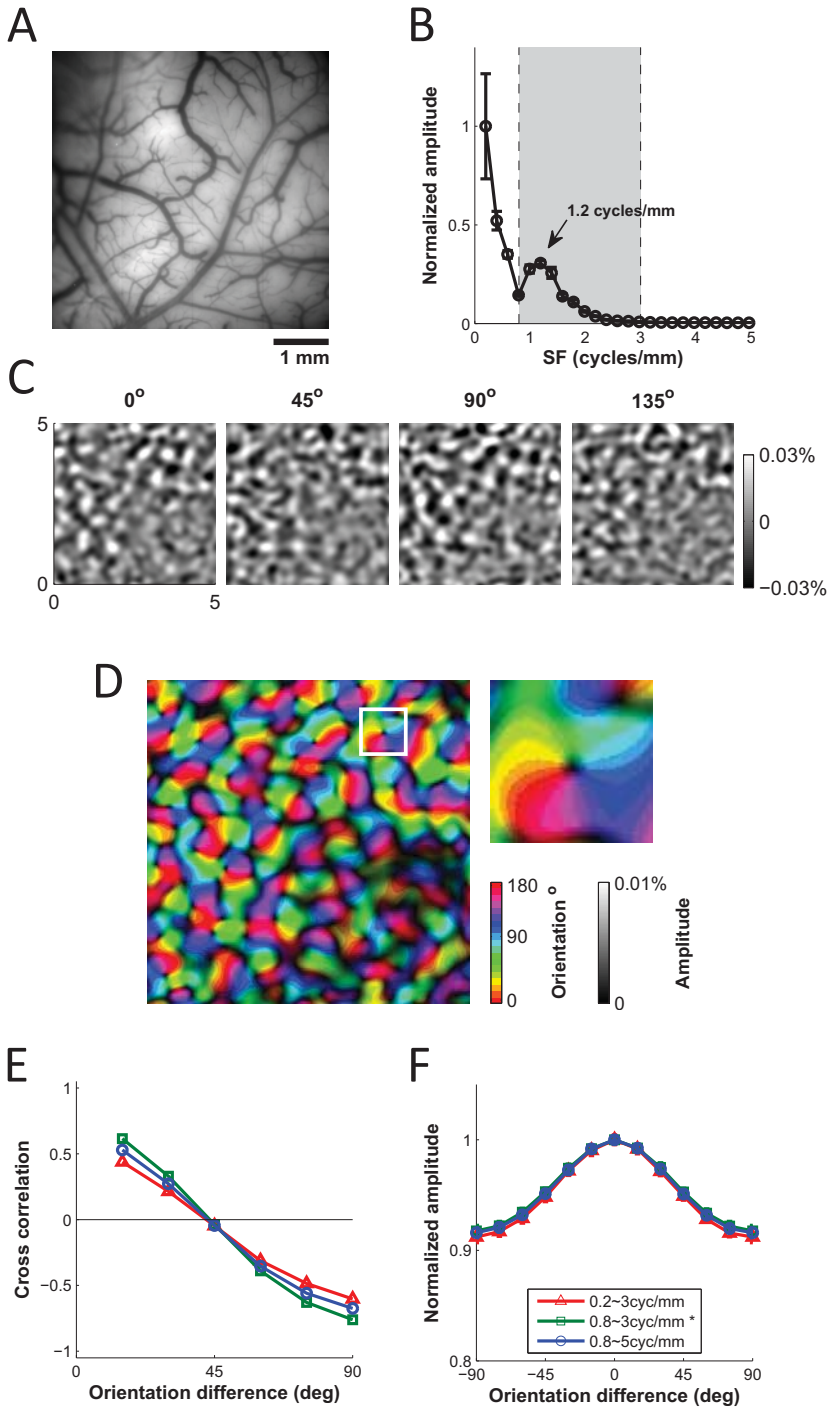
A
1 mm
B
Normalized amplitude
1.2 cycles/mm
SF (cycles/mm)
C
0°
45°
90°
135°
0.03%
0
−0.03%
D
180
90
0
Orientation °
0.01%
0
Amplitude
E
Cross correlation
Orientation difference (deg)
F
Normalized amplitude
0.2~3cyc/mm
0.8~3cyc/mm *
0.8~5cyc/mm
Orientation difference (deg)

Fig. 7

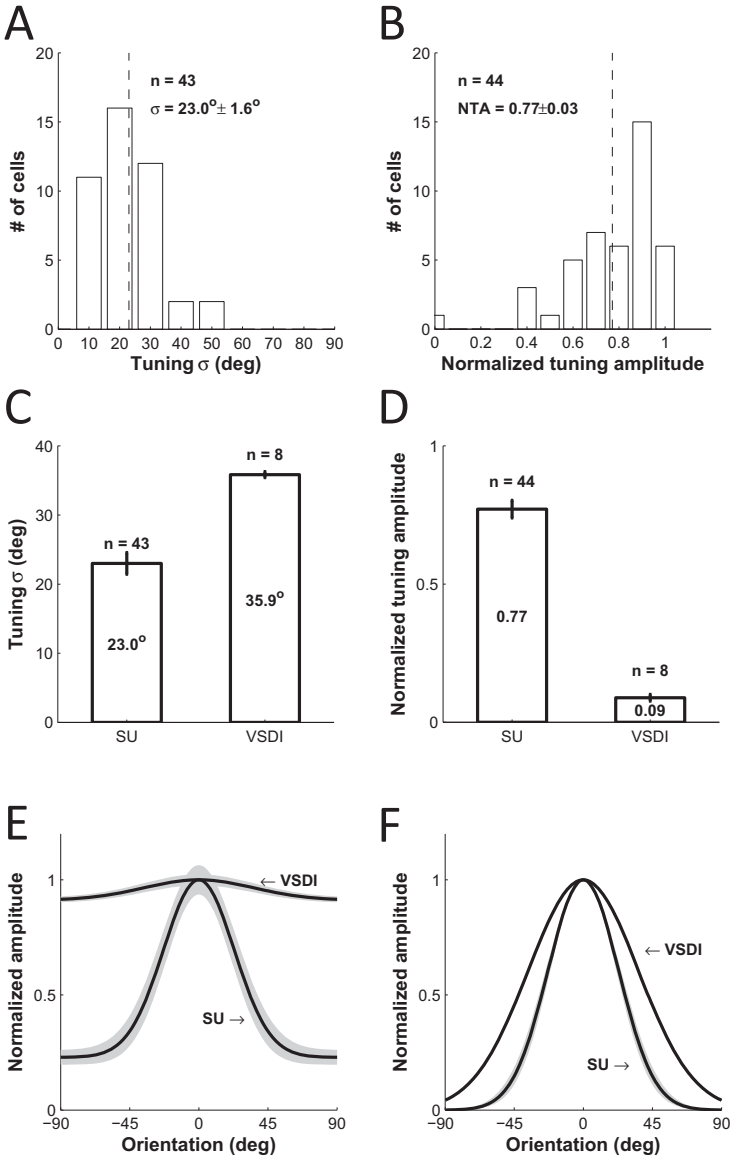
A
n = 43
σ = 23.0°± 1.6°
# of cells
Tuning σ (deg)
B
n = 44
NTA = 0.77±0.03
# of cells
Normalized tuning amplitude
C
n = 43
n = 8
23.0°
35.9°
Tuning σ (deg)
SU
VSDI
D
n = 44
n = 8
0.77
0.09
Normalized tuning amplitude
SU
VSDI
E
← VSDI
SU →
Normalized amplitude
Orientation (deg)
F
← VSDI
SU →
Normalized amplitude
Orientation (deg)

Fig. 8

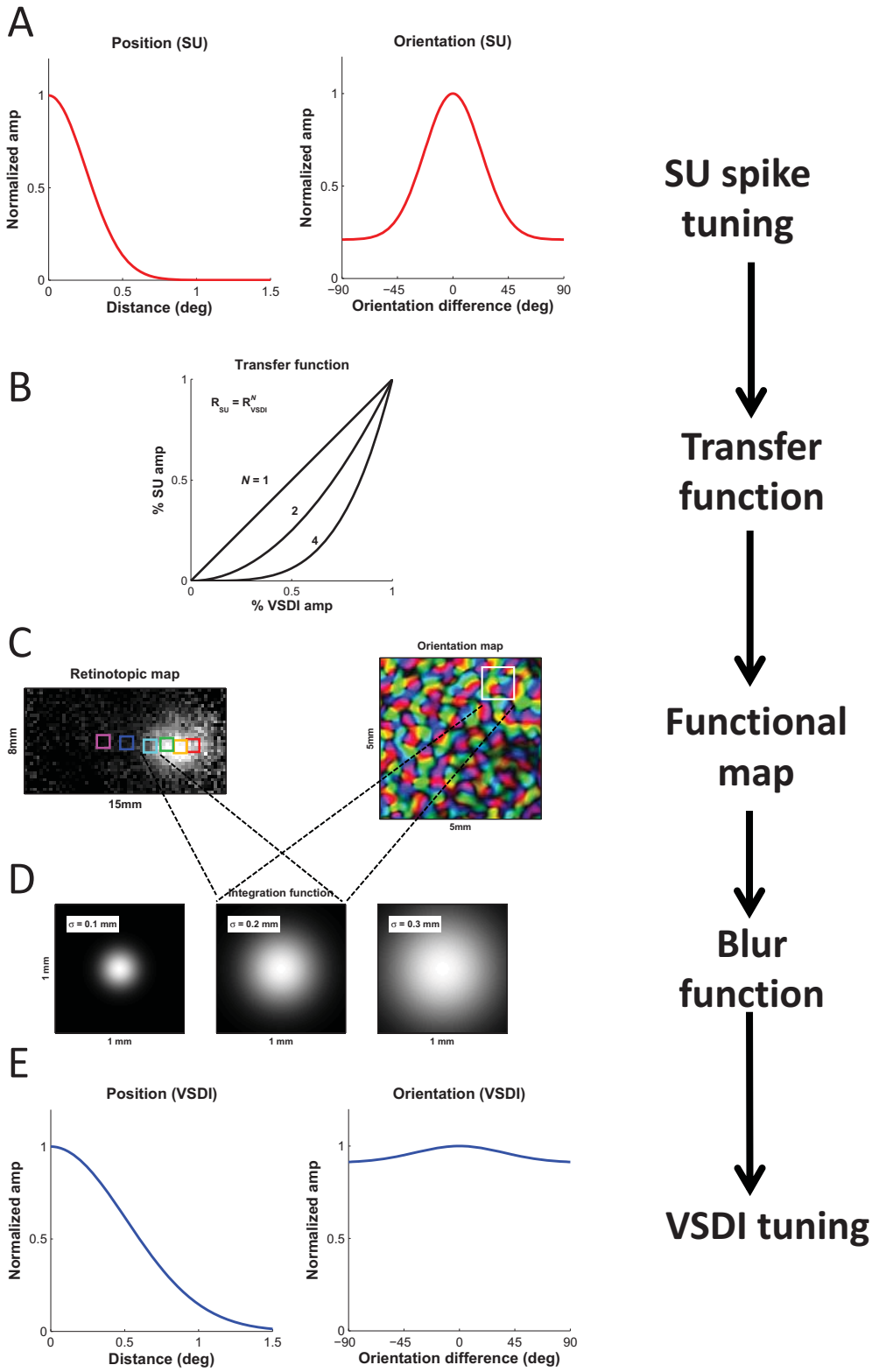
A
Position (SU)
Normalized amp
Distance (deg)
Orientation (SU)
Orientation difference (deg)
B
Transfer function
% SU amp
% VSDI amp
N = 1
2
4
C
Retinotopic map
8mm
15mm
Orientation map
5mm
5mm
D
Integration function
σ = 0.1 mm
σ = 0.2 mm
σ = 0.3 mm
1 mm
E
Position (VSDI)
Orientation (VSDI)
SU spike tuning
Transfer function
Functional map
Blur function
VSDI tuning

Fig. 9

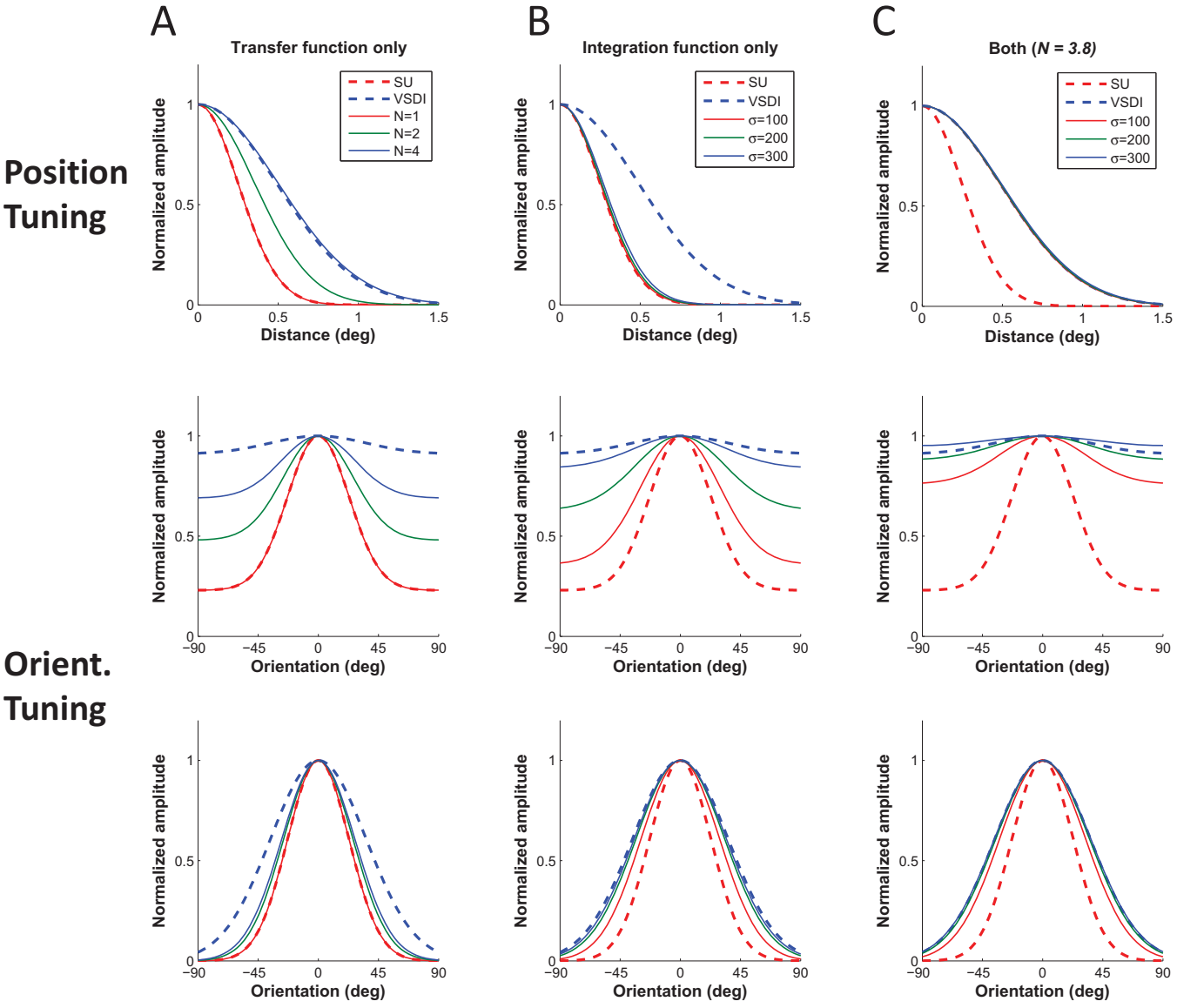
A
B
C
Transfer function only
Integration function only
Both (N = 3.8)
Position Tuning
Orient. Tuning
SU
VSDI
N=1
N=2
N=4
σ=100
σ=200
σ=300
Normalized amplitude
Distance (deg)
Orientation (deg)

Fig. 10

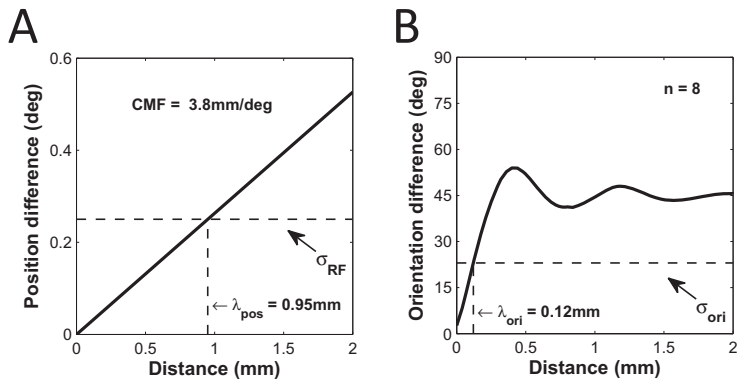
A
B
CMF = 3.8mm/deg
Position difference (deg)
Distance (mm)
σRF
← λpos = 0.95mm
n = 8
Orientation difference (deg)
Distance (mm)
← λori = 0.12mm
σori
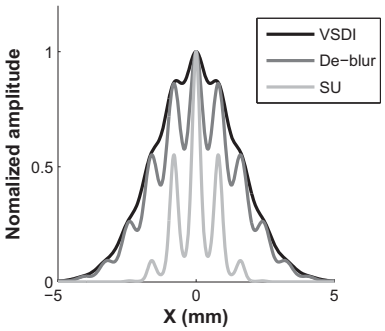
Fig. 11